TITLE: The Effect of Local Geometry and Relative Energy on Grain Boundary Area Changes During Grain Growth in $SrTiO_3$

AUTHORS: Vivekanand Muralikrishnan[1], Zipeng Xu[1], Gregory S. Rohrer[1], Amanda R. Krause[1*]

[1]Carnegie Mellon University, Pittsburgh PA

*Corresponding Author: amandakr@andrew.cmu.edu

JOURNAL: Journal of the American Ceramic Society

KEYWORDS: microstructure, $SrTiO_3$, high energy x-ray diffraction microscopy, grain growth

Published in the Journal of the American Ceramic Society.

http://dx.doi.org/10.1111/jace.20319

Abstract

This study utilizes high-energy x-ray diffraction microscopy of $SrTiO_3$ to identify correlations between grain boundary (GB) area changes and the motion direction of neighboring GBs to investigate interfacial energy minimization mechanisms during grain growth. The local GB area changes were measured near triple lines (TLs) to isolate the effects of neighboring GBs. These area changes were then correlated to the migration direction and curvature of the neighboring GBs present at the TL, providing an alternative metric associated with lateral expansion for describing GB migration. Additionally, this study extracted GB dihedral angles, which reflect the relative GB energy, to test whether low energy GBs replace high energy GBs (i.e., GB replacement mechanism) and, thus, can be used to predict a GB's migration direction. The majority of GBs did not exhibit local area changes reflective of the GB replacement mechanism, and the dihedral angles were not reliable indicators for GB motion. However, the expansion and shrinkage of GBs moving away from their center of curvature was more often consistent with the grain boundary replacement mechanism. These results suggest that growth for certain GB configurations is governed by relative energy differences while others are governed by curvature.

Introduction

The microstructure of a metal oxide affects its mechanical [1] and electrical [2–4] properties. Hence, efficient microstructural design is essential for tailoring material performance. However, grain growth is still challenging to control or predict during processing. In the classical description of grain boundary (GB) migration, GBs move toward their center of curvature, and their velocity is product of their reduced mobility and curvature [5–8]. However, recent experimental observations of GB migration using non-destructive 3D high energy x-ray diffraction microscopy (HEDM) in Ni [9], Fe [10], and $SrTiO_3$ [11] polycrystals are not consistent with that description. Instead, they show (1) individual GB velocity is not linearly correlated with curvature, and (2) GBs do not always migrate towards their center of curvature. These observations suggest that the mechanism governing local GB migration is not well understood.

Most polycrystalline materials have anisotropic GB energy, such that neighboring GBs having competing driving forces to increase or decrease their areas that complicates their motion. As discussed in the work by Niño and Johnson [12], interfacial energy minimization during grain growth can occur by a combination of mechanisms, including:

1) total GB area reduction,

2) low energy GBs replace high energy GBs (GB energy replacement mechanism), and

3) GBs reorientation to a lower energy state.

By comparing simulations of grain growth with isotropic and anisotropic GB energy, Niño and Johnson report that area reduction is the dominant energy dissipation mechanism. However, indirect and direct observations find that, as the total GB area decreases, low energy GBs on average increase in relative area and high energy GBs decrease in relative area in both experiments [10,13–16] and simulations with anisotropic GB energy [17–22]. Notably, HEDM observations in

Ni by Xu et al. [13] showed direct illustrations of low energy GBs expanding at the expense of their higher energy GB neighbors. Due to these observations, Xu et al. [10,13] hypothesized that the GB replacement mechanism may be responsible for the anti-curvature GB motion observed in polycrystals. The purpose of this study is to determine if the expansion of relatively low energy GBs is associated with anti-curvature motion using HEDM measurements of grain growth in $SrTiO_3$.

To test this idea, this work first explores how the local area changes of a GB at a triple line (TL) correlates with the motion direction of its direct neighbors. It is expected that the growth of a grain can be described by the area reduction of the adjacent GBs. Similarly, a GB should expand in area if it neighbors a shrinking grain. However, since a single GB touches many other grains, this study isolates the GB area changes around TLs. Then, the local GB area change is correlated to the dihedral angles at the TL, which provide a relative GB energy measurement, to test whether low energy GBs expand and high energy GBs shrink.

Only TLs with the topologies shown in Fig. 1 are investigated for simplicity. The convex and concave topologies introduced in Fig. 1 are classified based on how neighboring GBs in the TL are curved with respect to a common GB of interest. In the convex topology (represented by *VEX*), a GB of interest neighbors two GBs with mean curvatures that are convex with respect to their shared grain. Conversely, in a concave topology (represented by *CAV*), a GB of interest is neighboring two GBs with mean curvatures that are concave with respect to their shared grain. In both topologies, the GB of interest can be flat or curved in either direction. Additionally, the TLs are classified by the motion of the GBs neighboring the GB of interest. Those in which the two neighboring GBs move towards their center of curvature are labeled *CC*, whereas those in which the two neighboring GBs move away from their center of curvature (anti-curvature) are labeled

AA. All other topologies or those in which the neighboring boundaries have mixed motion (one moves towards its center of curvature and the against) are ignored for simplicity.

This analysis will compare the local area changes for the TL migration configurations. Then, the local GB area changes will be correlated to the initial GB dihedral angles. This analysis will potentially allow us to gain insights into the free energy minimization occurring during grain growth when GBs are bounded by GBs migrating towards their center of curvature and anti-curvature GBs.

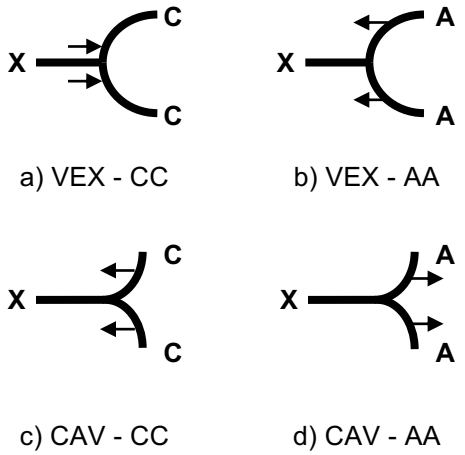

Figure 1: Schematic representation of the four TL configurations tested. The GB of interest is indicated with an *X*. *C* and *A* represent GBs moving towards or away from their center of curvature, respectively. The motion direction of these GBs is indicated by the arrows. If *X* GB is bounded by a (a, b) convex 'grain' (*VEX*), *X* is expected to expand and shrink if neighboring (a) *CC* and (b) *AA* GBs, respectively. Conversely, if *X* GB is bounded by a (c, d) concave 'grain' (*CAV*), *X* is expected to shrink and expand if neighboring (c) *CC* and (d) *AA* GBs, respectively. The GB can be flat or curved in either direction.

Methods

Material Processing and HEDM Data Collection

The detailed processes for the sample preparation, data collection, reconstruction and post-processing for $SrTiO_3$ HEDM data is described in an earlier publication [11]. Here, we will briefly describe the relevant sample details.

The bulk $SrTiO_3$ samples provided by Karlsruhe Institute of Technology were prepared by a solid-state synthesis route described in Ref [23]. To reach a reasonable grain size for characterization, the sintered sample was annealed at 1400°C for 10 h under flowing forming gas, after which the first HEDM map was collected. Then, the same sample was annealed in forming gas for an additional 70 h at 1400°C before the second HEDM measurement.

The HEDM maps were collected using the 1-ID beamline in the Argonne Photon Source at Argonne National Laboratory [24]. The diffraction data was reconstructed using the HEXOMAP software [25], and the reconstructed data was imported into Dream3D (an open-source software) [26] for subsequent grain segmentation and post-processing steps as discussed below.

Grains were segmented by grouping contiguous voxels with a misorientation threshold of 1°. The voxel dimensions are 2 μm × 2 μm × 2 μm. Grains with fewer than 16 voxels were removed, and their voxels were distributed to neighboring grains in a dilation process. Similarly, grain dilation was performed to remove pores (unindexed regions) with fewer than four voxels.

GB velocity, area, curvature, and dihedral angles calculations

To calculate GB velocity, grains were matched between the two measurements and the HEDM maps were aligned spatially. Grains were matched by finding pairs with similar misorientation (< 1.5°) and centroid location (< 20μm). The microstructures are aligned by translating the second map by the average difference in centroid location between the matched

grains. The GB velocity is determined by calculating the net volume of voxels flipped across the GB divided by the initial GB area.

GB area is determined by summing the area of all the voxel faces present at the GB of interest or within the volume of interest. GB curvatures and dihedral angles were calculated from the first collected HEDM map, before the observed growth. GB mean curvature is determined by calculating the integral mean curvature and dividing by the initial GB area. Instead of smoothing or meshing the GB, the integral mean curvature (M_s) is computed for the voxelated structure, as described in Ref [27], using the equation below.

$$M_s = \frac{\pi}{4}(N_{outies} - N_{innies}) \quad (1)$$

where N_{outies} is the total number of edges formed by convex voxel faces, and N_{innies} is the total number of edges formed by concave voxel faces at the GB of interest.

To calculate the GB dihedral angle, Matlab's MTEX package was used to extract the TL points' coordinates for each layer of the 3D microstructure map and the GB tangent vector near the TL in each layer. The GB tangent vector was obtained after Laplacian smoothing the microstructure map of each layer for 25 iterations. The GB normal vector near the TL was obtained by calculating the cross product of the TL line vector with the GB tangent vector found. Then, the GB dihedral angles for the specific TL were calculated from the dot product of the GB normal vectors. The GB dihedral angle reported is the average value of those calculated at each layer containing the TL.

Calculation for local GB area change

The local GB area change near a TL is calculated by the difference in GB area between the first and second HEDM maps within a constrained volume that contains the initial and final TL position (see Fig. 2). Considering both positions in both timesteps, the minimum and maximum *x*,

y, and *z* coordinates of the two TL were identified. The bounds of the constrained volumes were set as the minimum and maximum coordinates, which were first rounded to the nearest integer and a single voxel was subtracted or added, respectively.

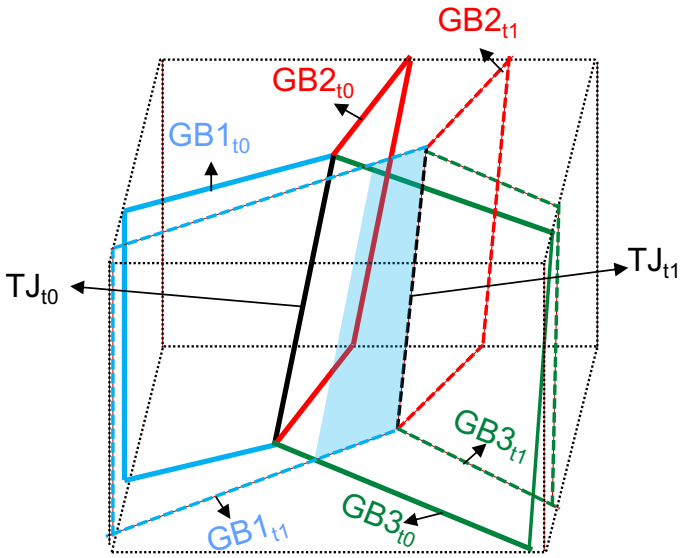

Figure 2: Schematic of constrained volume containing TL found before (t0, GBs bounded by solid lines) and after annealing (t1, GBs bounded by dashed lines) that is used for calculating local area changes. The local area change of GB1 (shaded in blue) is determined by the difference in GB area of the $GB1_{t1}$ and $GB1_{t0}$ within the constrained volume. Note that the end points of the TL are not included in the schematic for simplicity but the entire TL is within the constrained volume for all calculations.

Classification and TL Selection Criteria

The GB's direction of motion is classified based on the sign of the GB velocity and the GB mean curvature product. If a GB moves towards its center of curvature (represented by *C*), the GB velocity and GB mean curvature have opposite signs with respect to the same reference grain such that their product is a negative value. Conversely, if a GB moves away from its center of curvature (anti-curvature GB motion, represented by *A*), the product of its velocity and curvature with respect

to the reference grain is greater than or equal to zero. Note, a product of zero is considered anti-curvature because it indicates the motion of a flat boundary or a stationary curved boundary.

The GB dihedral angle and local area changes are compared for four different configurations shown in Fig. 1: GBs bounded by concave GBs that either both moved towards their center of curvature (*CAV-CC*) or against their center of curvature (*CAV-AA*) and GBs bounded by convex GBs that either moved towards their center of curvature (*VEX-CC*) or against their center of curvature (*VEX-AA*). Table 1 reports the number of GBs used for the GB dihedral angle and local GB area change distributions for the different configurations tested.

Table 1: The number of GBs used in the dihedral angle and local area change for the four different configurations in Fig. 1. Note that the GB of interest may be *A* or *C* and the curvature is not constrained.

VEX or CAV	CC or AA	Number of GBs
VEX	CC	935
VEX	AA	623
CAV	CC	1003
CAV	AA	653

Results and Discussion

Figure 3 compares the local GB area changes for the different configurations tested. On average, when the GBs are bounded by GBs migrating towards their center of curvature (*CC*, black curves in Fig. 3), the *X* GBs with *VEX* topology increase in area and the *X* GBs with *CAV* topology decrease in area. The GBs bounded by anti-curvature GBs (*AA*, red curves in Fig. 3) show the opposite trends; on average, the *X* GBs with *VEX* topology decrease in area and the *X* GBs with *CAV* topology increase in area. Note that the magnitude of area changes is greater for the *X* GBs neighboring *CC* GBs than those neighboring *AA* GBs, irrespective of topology.

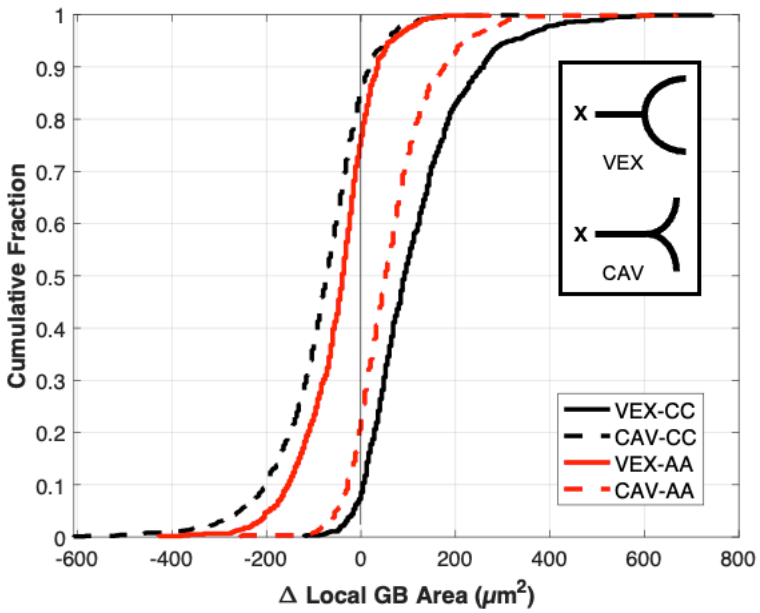

Figure 3: Cumulative distribution of the change in the local GB area for the four TL configurations introduced in Fig. 1.

Figure 3 shows that, on average, the local area change of a GB is related to the curvature and direction of motion of the neighboring GBs. For example, a GB is likely to expand if it neighbors a shrinking convex grain. Alternatively, the GB likely shrinks if its neighbor is a growing convex grain (anti-curvature motion). (Similar arguments can be made for GBs neighboring concave grains as shown in Figs. 3.) This relationship holds for 83% of the GBs in this study, suggesting that the GB's lateral growth is important for elucidating the migration behavior. (Note that the GB's area change is also dependent on the motion of adjacent TLs and its own migration, which may account for those GBs not conforming to this relationship.) If the GB replacement mechanism dominates, the inverse relationship would be true; the expansion of a low energy GB locally would cause the neighboring grain to shrink whether it be convex (following curvature) or concave (anti-curvature motion).

To test whether the observed correlation reflects the GB replacement mechanism, the dihedral angle distributions were used to classify GB energy. The GB dihedral angles are inversely related to the GB energy based on the Young's equation [28] below.

$$\frac{\gamma_1}{\sin\theta_1} \equiv \frac{\gamma_2}{\sin\theta_2} \equiv \frac{\gamma_3}{\sin\theta_3} \quad (2)$$

γ_1, γ_2, and γ_3 are the GB energy and θ_1, θ_2, and θ_3 are the corresponding GB dihedral angles of the three GBs meeting at the TL. This equation was derived based on the force equilibrium of the GBs at the TL and ignores any variation in the GB energy with GB plane orientation. It is important to note that the dihedral angle is providing the relative GB energy with respect to the neighbors present at that same TL. The absolute energy or the relative GB energy to the entire GB population is not known. However, since this study is concerned with the local migration behavior, dihedral angles are useful to determine whether a GB should want to expand or shrink given their neighborhood.

The dihedral angle distributions suggest that the relative GB energy and topology are correlated. Figure 4 and Table 2 compare the dihedral angle cumulative distributions and averages, respectively, for the different TL configurations. On average, GBs bounded by *VEX* GBs (solid lines in Fig. 4) have a lower GB dihedral angle than GBs bounded by *CAV* GBs (dashed lines in Fig. 4), irrespective of the different boundary migration conditions. Two sample Kolmogorov – Smirnov (KS) tests show that these distributions are statistically different (p-value << 0.05) when GBs have different GB topologies (Table 3). These results support the conclusion that GBs bounded by *VEX* GBs, on average, have a higher relative GB energy than their neighbors and GBs bounded by *CAV* GBs have lower relative GB than their neighbors.

In contrast to a previous study of grain boundaries in $SrTiO_3$ [29], the sample did not exhibit a strong anisotropy in the grain boundary plane or energy distributions. This is thought to

reflect the difference on the partial pressure of oxygen during preparation (air in the previous work and forming gas here). Nevertheless, the dihedral angle distributions show systematic differences suggesting that the grain boundary energies cannot be considered isotropic, even if the variations are smaller than in previously studied materials.

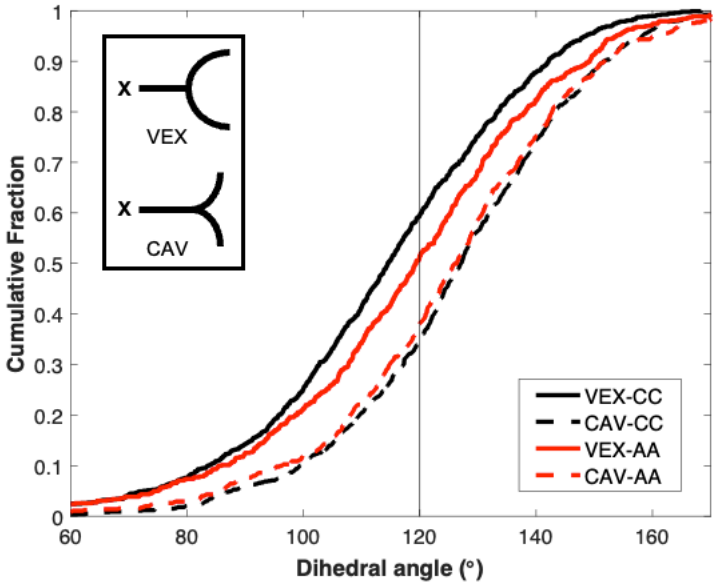

Figure 4: Cumulative distributions of dihedral angles for the four configurations introduced in Fig. 1. These measurements were collected from the first HEDM map.

Table 2: The mean dihedral angle for GBs bounded by the different configurations.

CAV or VEX	CC or AA	Mean GB Dihedral Angle
VEX	CC	114°
VEX	AA	118°
CAV	CC	126°
CAV	AA	125°

Table 3: The p-values calculated from two sample Kolmogorov Smirnov (KS) test comparing all possible combinations of the four configurations. The p-values less than 0.05, highlighted in grey, indicate the distributions are statistically different.

GB topology – TL migration configuration pairs for KS test		p-value
VEX-CC	VEX-AA	7×10^{-4}
CAV-CC	CAV-AA	0.5413
VEX-CC	CAV-CC	4×10^{-28}
VEX-CC	CAV-AA	2×10^{-18}
VEX-AA	CAV-CC	5×10^{-10}
VEX-AA	CAV-AA	7×10^{-6}

According to the GB replacement mechanism hypothesis, the GBs bounded by *CAV* GBs are expected to increase in area because they are in general lower in energy relative to their neighbors. However, GBs bound by *CAV-CC* shrink on average. Similarly, the higher energy GBs (those bounded by *VEX* GBs) expand in area as their neighboring GBs move towards their center of curvature. These results indicate that factors other than the relative grain boundary energy, including geometrical constraints and curvature, influence grain boundary migration. Furthermore, these cases represent classes of triple lines where the local geometry is more influential than the relative energy.

In contrast, when bounded by anti-curvature boundaries (*AA*), lower energy GBs are more likely to expand and high energy GBs are more likely to shrink. This can be seen by the GBs bounded by *CAV*, which is associated with lower energy, increasing in area. Similarly, GBs bounded by *VEX* GBs, which is the topology associated with higher energy, on average decrease in local area. Thus, for these classes of TLs, the relative energy is more important than local geometry in determining grain boundary migration.

This trend for TLs with *AA* boundaries is not held when classifying GBs by their dihedral angles rather than topology; only half of GBs bounded with anti-curvature boundaries with dihedral angles greater than 120° and those with less than 120° increase and decrease, respectively,

in local area. Figure 5 shows that the dihedral angle does not predict the expansion or shrinkage of a GB irrespective of the motion of its neighbors or topology. The GBs with the configuration associated with the lowest dihedral angles (*VEX-CC*, Fig. 4) are more likely to expand rather than shrink and their neighbors move towards their center of curvature. Therefore, the dihedral angles, like curvature, cannot be used as an indicator of local GB area change or the motion direction of neighboring GBs.

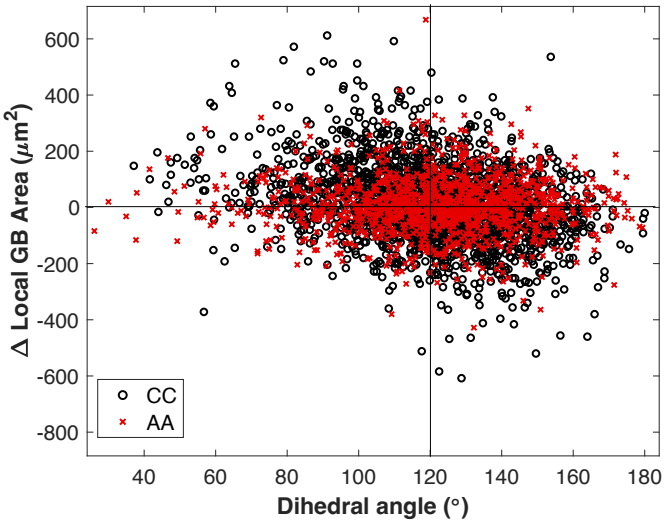

Figure 5: The change in local area for each grain boundary plotted with respect to its dihedral angle.

This study finds that geometry (i.e., curvature) or relative energy governs motion for different classes of TLs. However, no clear indicator was found to identify which GBs will be dominated by relative energy instead of geometry. It is expected that GB replacement would dominate when the absolute difference in energy between neighboring GBs is high. Although providing energy information, the dihedral angles may not be indicative because they reflect the energy ratio rather than the absolute energy difference. For a given energy ratio, the absolute difference in energy can vary significantly depending on the minimum GB energy present. Given that $SrTiO_3$ is a polycrystalline ceramic primarily composed of general, high-angle GBs, the

probability of a high energy GB neighboring two low energy GBs is low and, thus, unlikely to be reflected in the dihedral angle measurement. Therefore, it is possible that anti-curvature motion is associated with TLs that have the greatest absolute energy difference or the removal of the highest energy GBs but not discernable from the measurements here.

Conclusions

This work aimed to gain insights into the free energy minimization mechanism when GBs migrate towards and against their center of curvature in $SrTiO_3$ polycrystals as measured with HEDM. First, the local change in GB area was correlated to the motion direction of its neighboring GBs, irrespective of their curvature. This method provides an alternative metric to describe GB migration in terms of lateral motion rather than the typical velocity term associated with GBs moving perpendicular to their plane. To test whether GB motion direction is also correlated to the expansion of its low energy GBs neighbors (or the shrinkage of its high energy GBs neighbors), the local area change was compared to the GB's dihedral angle, which was used as an indicator of its relative GB energy. On average, anti-curvature motion is associated with the expansion of lower energy GBs and the shrinkage of higher energy GBs. However, most GBs investigated in this study do not show the relationship between the area change and the dihedral angle that is expected if GB replacement mechanisms were to dominate. Furthermore, individual dihedral angles, like curvatures, cannot be used as an indicator of local GB migration directions. Because the full GB energy function is not known, the analysis is limited to only consider relative GB energy between neighbors and cannot isolate the behavior of truly low or high energy GBs, which may have an outsized role on the energy dissipation mechanism.

Acknowledgements

This work was supported by the National Science Foundation under DMREF Grant No. 2118945. The Advanced Photon Source is a US Department of Energy (DOE) Office of Science User Facility operated for the DOE Office of Science by Argonne National Laboratory under contract no. DE-AC02–06CH11357.

References

1. Bokov A, Zhang S, Feng L, Dillon SJ, Faller R, Castro RHR. Energetic design of grain boundary networks for toughening of nanocrystalline oxides. J Eur Ceram Soc. 2018 Sep;38(12):4260–7.

2. Tan Y, Zhang J, Wu Y, Wang C, Koval V, Shi B, Ye H, McKinnon R, Viola G, Yan H. Unfolding grain size effects in barium titanate ferroelectric ceramics. Sci Rep. 2015 May 7;5(1):9953.

3. Luo J. Interfacial engineering of solid electrolytes. J Materiomics. 2015 Mar;1(1):22–32.

4. Wang Z, Cao M, Yao Z, Li G, Song Z, Hu W, Hao H, Liu H, Yu Z. Effects of Sr/Ti ratio on the microstructure and energy storage properties of nonstoichiometric SrTiO3 ceramics. Ceram Int. 2014 Jan;40(1):929–33.

5. Burke JE, Turnbull D. Recrystallization and grain growth. Prog Met Phys. 1952 Jan;3:220–92.

6. Gottstein G, Shvindlerman LS. On the true dependence of grain boundary migration rate on driving force. Scr Metall Mater. 1992 Dec;27(11):1521–6.

7. Mullins WW. Two-Dimensional Motion of Idealized Grain Boundaries. J Appl Phys. 1956 Aug 1;27(8):900–4.

8. Smith CS. Grain Shapes and Other Metallurgical Applications of Topology. Metallogr Microstruct Anal. 2015 Dec;4(6):543–67.

9. Bhattacharya A, Shen YF, Hefferan CM, Li SF, Lind J, Suter RM, Krill CE, Rohrer GS. Grain boundary velocity and curvature are not correlated in Ni polycrystals. Science. 2021 Oct 8;374(6564):189–93.

10. Xu Z, Shen YF, Naghibzadeh SK, Peng X, Muralikrishnan V, Maddali S, Menasche D, Krause AR, Dayal K, Suter RM, Rohrer GS. Grain boundary migration in polycrystalline α-Fe. Acta Mater. 2024 Jan;264:119541.

11. Muralikrishnan V, Liu H, Yang L, Conry B, Marvel CJ, Harmer MP, Rohrer GS, Tonks MR, Suter RM, Krill CE, Krause AR. Observations of unexpected grain boundary migration in SrTiO3. Scr Mater. 2023 Jan;222:115055.

12. Niño JD, Johnson OK. Influence of grain boundary energy anisotropy on the evolution of grain boundary network structure during 3D anisotropic grain growth. Comput Mater Sci. 2023 Jan;217:111879.

13. Xu Z, Hefferan CM, Li SF, Lind J, Suter RM, Abdeljawad F, Rohrer GS. Energy dissipation by grain boundary replacement during grain growth. Scr Mater. 2023 Jun;230:115405.

14. Bojarski SA, Ma S, Lenthe W, Harmer MP, Rohrer GS. Changes in the Grain Boundary Character and Energy Distributions Resulting from a Complexion Transition in Ca-Doped Yttria. Metall Mater Trans A. 2012 Oct;43(10):3532–8.

15. Muralikrishnan V, Langhout J, Delellis DP, Schepker K, Krause AR. Engineering grain boundary energy with thermal profiles to control grain growth in $SrTiO_3$. J Am Ceram Soc. 2024 Jul 8;jace.19982.

16. Saylor DM, Morawiec A, Rohrer GS. The relative free energies of grain boundaries in magnesia as a function of five macroscopic parameters. Acta Mater. 2003 Aug;51(13):3675–86.

17. Kar D, Sintay SD, Rohrer GS, Rollett AD. Role of Inclination Dependent Anisotropy on Boundary Populations during Two-Dimensional Grain Growth. Mater Sci Forum. 2012 Apr;715–716:697–702.

18. Holm E, Hassold GN, Miodownik MA. On misorientation distribution evolution during anisotropic grain growth. Acta Mater. 2001 Sep 3;49(15):2981–91.

19. Liu X, Wang J. Low-energy, Mobile Grain Boundaries in Magnesium. Sci Rep. 2016 Feb 19;6(1):21393.

20. Gruber J, George DC, Kuprat AP, Rohrer GS, Rollett AD. Effect of anisotropic grain boundary properties on grain boundary plane distributions during grain growth. Scr Mater. 2005 Aug;53(3):351–5.

21. Salama H, Kundin J, Shchyglo O, Mohles V, Marquardt K, Steinbach I. Role of inclination dependence of grain boundary energy on the microstructure evolution during grain growth. Acta Mater. 2020 Apr;188:641–51.

22. Naghibzadeh SK, Xu Z, Kinderlehrer D, Suter R, Dayal K, Rohrer GS. Impact of grain boundary energy anisotropy on grain growth. Phys Rev Mater. 2024 Sep 19;8(9):093403.

23. Bäurer M, Kungl H, Hoffmann MJ. Influence of Sr/Ti Stoichiometry on the Densification Behavior of Strontium Titanate. J Am Ceram Soc. 2009 Mar;92(3):601–6.

24. Lienert U, Li SF, Hefferan CM, Lind J, Suter RM, Bernier JV, Barton NR, Brandes MC, Mills MJ, Miller MP, Jakobsen B, Pantleon W. High-energy diffraction microscopy at the advanced photon source. JOM. 2011 Jul;63(7):70–7.

25. Liu H, Suter R. HEXOMAP: High Energy X-ray Orientation Mapping [Internet]. 2023 [cited 2023 Jun 24]. Available from: https://github.com/HeLiuCMU/HEXOMAP

26. Groeber MA, Jackson MA. DREAM.3D: A Digital Representation Environment for the Analysis of Microstructure in 3D. Integrating Mater Manuf Innov. 2014 Dec;3(1):56–72.

27. Patterson B, DeHoff R, Sahi C, Sun J, Oddershede J, Bachmann F, Lauridsen E, Jensen DJ. Integral mean curvature analysis of 3D grain growth: Linearity of dV/dt and grain volume. IOP Conf Ser Mater Sci Eng. 2019 Aug 1;580(1):012020.

28. Smith C. Grains, phases, and interfaces—an interpretation of microstructure. Trans AIME. 1948;175:15–51.

29. Zhong X, Kelly MN, Miller HM, Dillon SJ, Rohrer GS. Grain boundary curvatures in polycrystalline SrTiO3: Dependence on grain size, topology, and crystallography. J Am Ceram Soc. 2019;102(11):7003–14.